Title

Selenium Fractionation and Cycling in ther Intertidal Zone of the Car quinez Strait - Quarterly Progress Report, April 1, 1996 - June 30, 1996

Author

Zawislanski, Peter T.

Publication Date

1996-07-01

LBNL-39617
UC-100

ERNEST ORLANDO LAWRENCE
BERKELEY NATIONAL LABORATORY

Selenium Fractionation and Cycling in the Intertidal Zone of the Carquinez Strait

Quarterly Progress Report April 1996 through June 1996

P. T. Zawislanski, S.M. Benson, A.A. Brownfield, S. Chau, E. Gabet, T.M. Johnson, D. King, A.E. McGrath, H.S. Mountford, S.C.B. Myneni, J. Oldfather, T.C. Sears, and H.-W.C. Wong

Earth Sciences Division

July 1996

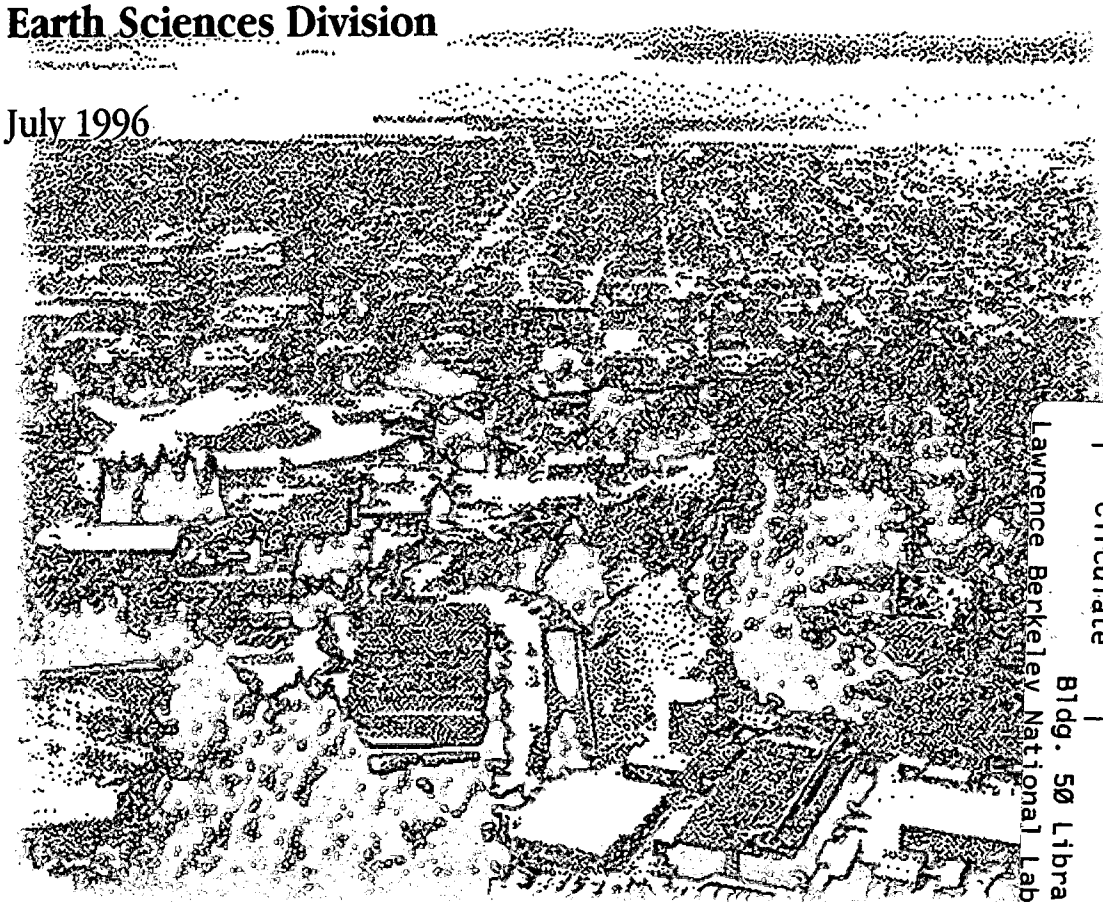

DISCLAIMER

LBNL - 39617
UC - 100

Selenium Fractionation and Cycling in the Intertidal Zone of the Carquinez Strait

Quarterly Progress Report
April 1996 through June 1996

P. T. Zawislanski, S. M. Benson, A. A. Brownfield, S. Chau, E. Gabet, T. M. Johnson, D. King, A. E. McGrath, H. S. Mountford, S. C. B. Myneni, J. Oldfather, T. C. Sears, H.-W. C. Wong

Earth Sciences Division
Lawrence Berkeley National Laboratory
University of Berkeley
Berkeley, California 94720

July 1996

This work was supported the San Francisco Bay Regional Water Quality Control Board, and by the Assistant Secretary for the Fossil Energy, Office of Oil, Gas and Shale Technologies, of the U.S. Department of Energy under Contract No. DE-AC03-76SF00098.

TABLE OF CONTENTS

1 INTRODUCTION

This quarterly report describes research on selenium (Se) cycling in the marshes and mudflats of the Carquinez Strait between 4/1/96 and 6/30/96. Chapter 2 contains descriptions of results of extractions and analyses of sediment cores from the intertidal zone of the Martinez and Benicia field sites, including Se fractionation data from Martinez Regional Park. Chapter 3 contains a summary of work in progress on the extraction of various Se species from sediment/soil samples, and efforts in measuring suspended sediment Se. Chapter 4 is an update on stable Se isotope research and Se purification techniques. Chapter 5 describes the recent developments in low-level Se analytical methods. Chapter 6 presents preliminary sedimentation rate data from the Martinez field site. Exciting new developments in x-ray spectroscopy of clams are presented in Chapter 7. The reader is referred to the 1995 Annual Report (Zawislanski et. al., 1995) for details on the project design, site selection, and methodology.

2 EXTRACTION AND ANALYSIS OF INTERTIDAL SEDIMENTS

Soil and sediment cores collected at both the Martinez Regional Park (MRP) site and the Southampton Bay (SHB) site in early December have been characterized, extracted and analyzed. Data presented herein are a sample of a very large data set on the dominant association of Se with various fractions in the sediment. The reader is referred to the previous two Quarterly Reports (Zawislanski et al., January 1996; April 1996) and the 1995 Annual Report (Zawislanski et. al., 1995) for details on sampling strategy and sediment characterization methods. Samples were collected from all of the major intertidal environments: mudflat, mudflat/marsh interface, lower marsh, and upper marsh. The spatial distribution of sample points at MRP is shown in Figure 2.1.

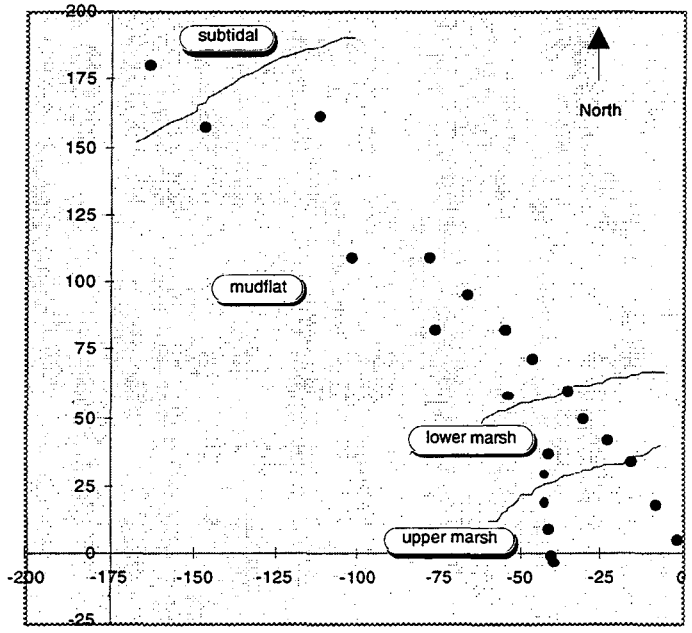

Figure 2.1 Location of core sampling points relative to the intertidal environments at MRP.

2.1 Chemical and Physical Characteristics of the Intertidal Zone

A very large data set of chemical and physical properties of the intertidal zone at both MRP and SHB has been compiled from the 20-cm cores. Being that not all data has been

fully analyzed, the goal of this report is to present the most important features and focus primarily on the MRP site. The following variables were measured: soil pH (Sb electrode) and Eh (Pt electrode); interstitial water pH, Eh, and electrical conductivity (EC); water extract pH, Eh, and EC; pore moisture content; total moisture content (pore+interstitial); elevation (indicative of degree of inundation); dry bulk density; organic carbon content; total selenium; dissolved Se in interstitial and extracted waters; "adsorbed" Se, as defined by a phosphate extract; "organically-associated" Se, as defined by a sodium hydroxide extract; "elemental", or zero-valent Se, as defined by a sodium sulfite extract; and "residual" Se, defined by the difference between total Se and the sum of all other fractions. Pyrite-Se has been measured on a small subset of samples and found to be negligible. The reasons for this require further investigation.

2.2.1 Field Variables Relevant to the Control of Se Speciation

Eh and pH are considered "master variables" which control the speciation of elements in the water-sediment system. In theory, and under presumed equilibrium conditions, the knowledge of these variables should allow one to predict the state of all species. However, in a system as complex as a wetlands sediment, which is subjected to frequent changes in moisture content, salinity, and organic influx, equilibrium is not expected, and the speciation of elements, and especially trace elements is very difficult to predict. Nonetheless, knowledge of the pH-Eh regime of various environments and the actual speciation of Se is helpful in understanding Se cycling in the intertidal zone.

Perhaps the least ambiguous of all measurements is that of the pore moisture content of the sediments. The distribution of moisture at site MRP (Transect 1) on 12/5/96 is shown in Fig. 2.2. There is a very apparent contrast between marsh and mudflat sediments, with the pore gravimetric moisture content as high as 1.9 g g^{-1} in the upper marsh and as low as 0.3 g g^{-1} in the mudflats. This is primarily related to the water retention capacity of the sediment, which in turn is related to bulk density and texture of the sediment. The dry bulk density of sediments in the upper marsh can be as low as 0.3 g cm^{-3}, while in the mudflats it approaches 1 g cm^{-3}. This is due to the finer texture and much higher organic carbon (OC) content of upper marsh sediments (shown in Fig. 2.3) and has important implications for redox conditions. Namely, even though the mudflats are inundated much more often than the upper marsh, the higher moisture retention capacity of marsh soils and much higher OC may result in equally or perhaps even more reducing conditions.

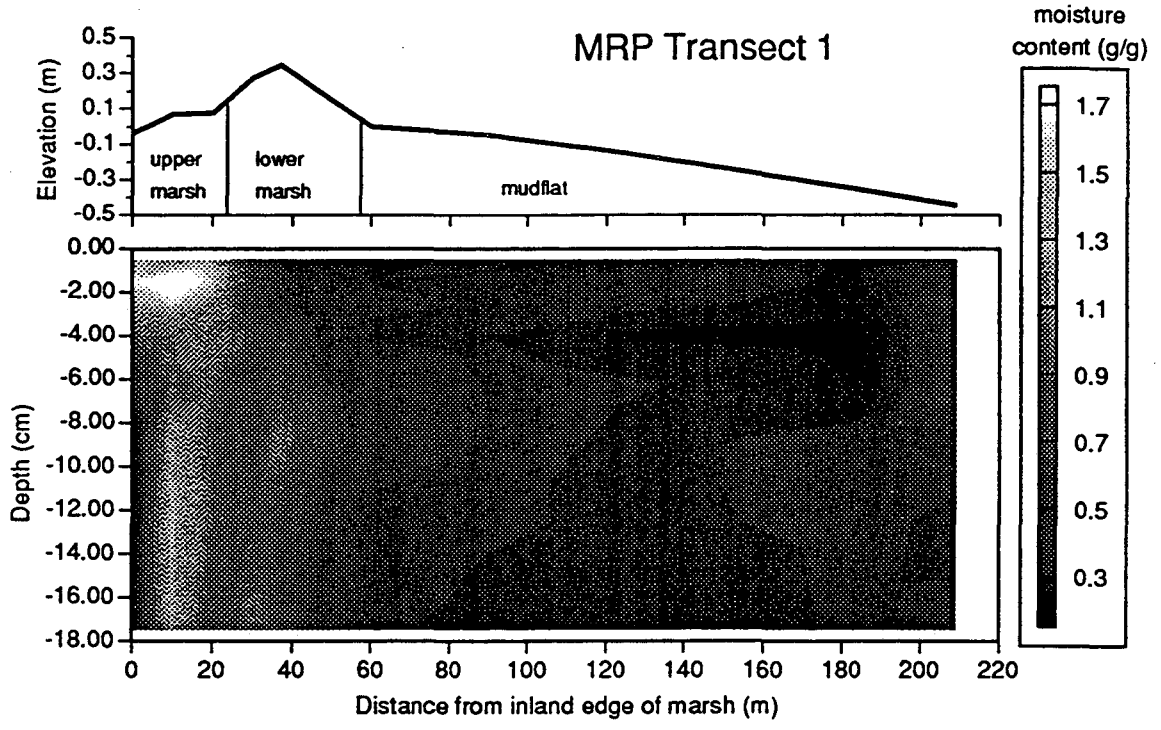

Figure 2.2 Pore gravimetric moisture content measured along Transect 1 at site MRP. The top graph shows the surface elevation of the transect.

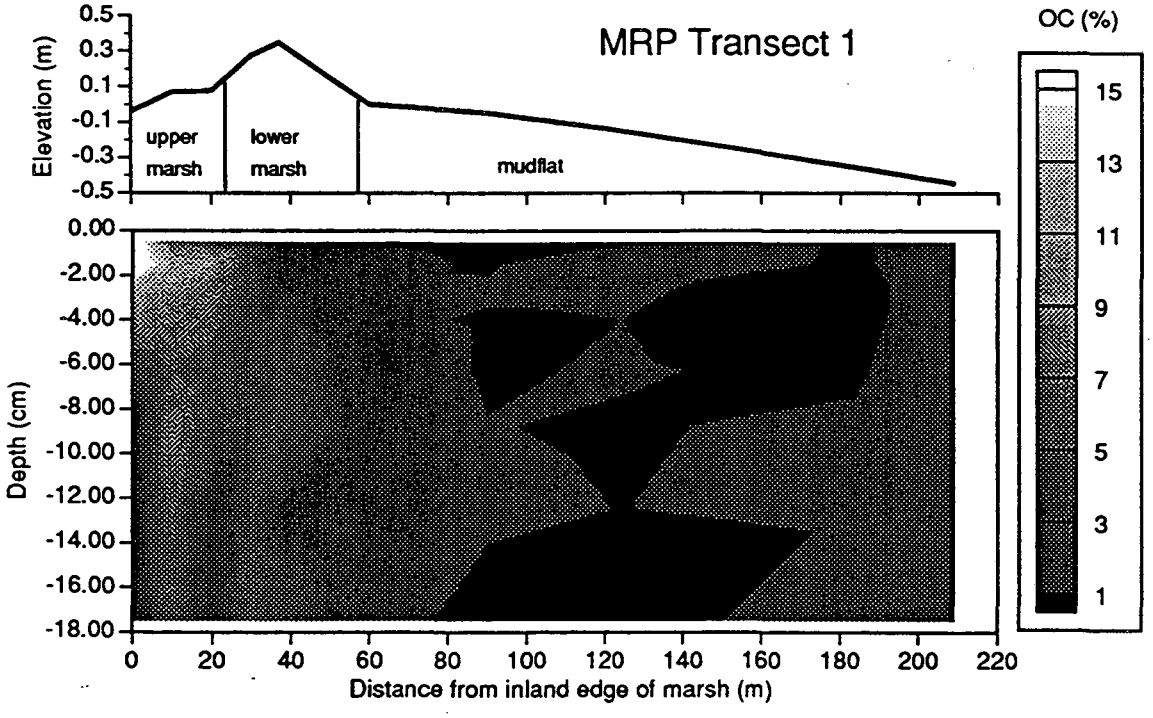

Figure 2.3 Organic carbon (OC) content measured along Transect 1 at site MRP. The top graph shows the surface elevation of the transect.

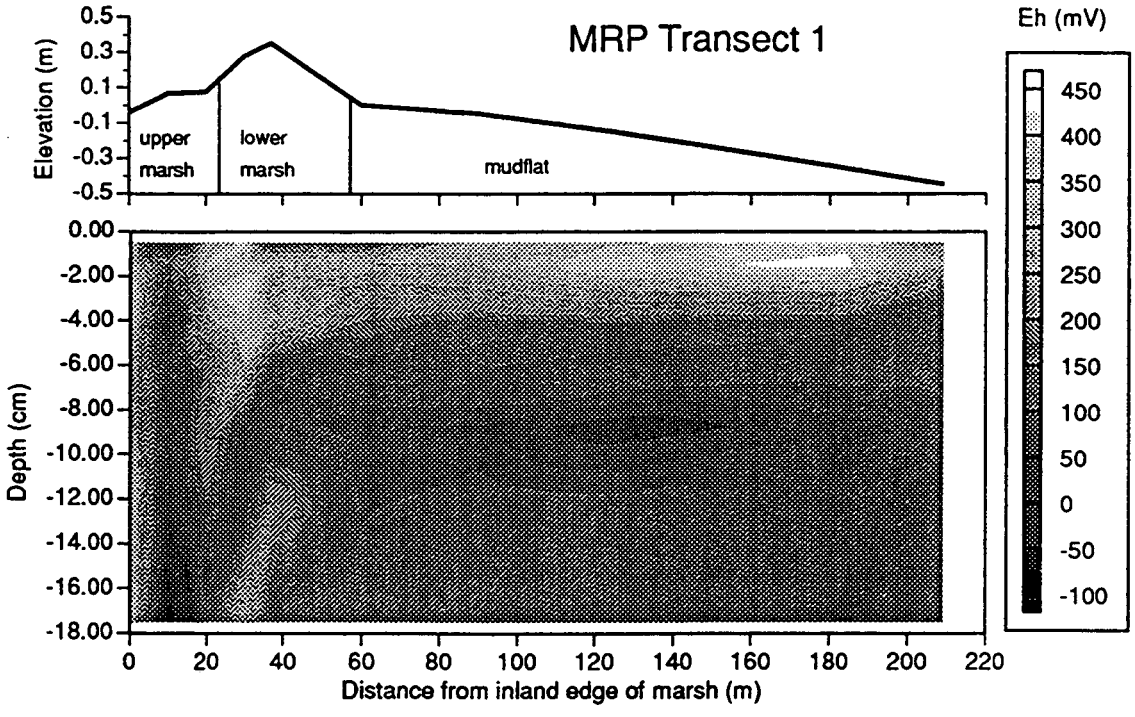

Figure 2.4 Redox potential, or Eh, measured along Transect 1 at site MRP. The top graph shows the surface elevation of the transect.

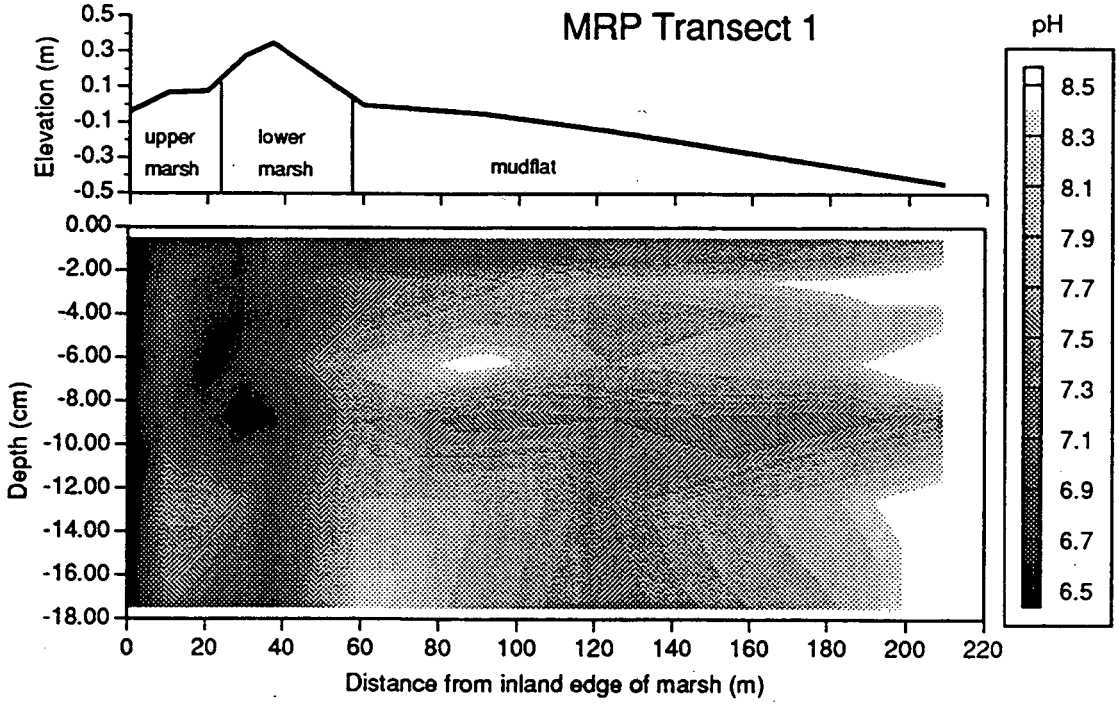

Figure 2.5 pH, measured along Transect 1 at site MRP. The top graph shows the surface elevation of the transect.

The redox potential, or Eh, of Transect 1 sediments, as measured directly on the core using Pt electrodes, is shown in Figure 2.4. The most important feature is the relatively narrow range of Eh. Although there are a few high and low outliers, most of the sediments fall in the 50 to 350 mV range. The Eh is generally well correlated with depth, with conditions more oxidized near the surface. Although Eh conditions are more heterogeneous in the marsh than in the mudflats, due to the presence of roots, overall Eh is higher in the mudflats, especially near the sediment surface. The pH of these sediments is shown in Figure 2.5 and displays a similar but opposite trend to Eh, with pH generally increasing with depth, but more dominated by local lows in the marsh, possibly as a result of root exudates. When both the Eh and pH are compared to a Se stability diagram, the area they define falls primarily in the elemental Se and selenite fields. Although this apparently limits Se speciation possibilities, Se *association* is not limited.

Sediment salinity is often an indicator of evapotranspirative processes which generally result in an accumulation of salts and associated trace elements. EC is an indirect, but representative measurement of salinity, and is shown in Figure 2.6. There is a clear trend of increasing salinity toward the upper marsh. This can be easily explained by the fact that the upper marsh is least frequently flooded and thickly vegetated and therefore most likely to be affected by evapotranspiration.

2.2.2 Selenium Fractionation

A description of total Se concentrations along Transect 1 at MRP (Figure 2.7) and a more detailed analysis thereof can be found in the April 1996 Progress Report. Data from Transect 2 is shown in Figure 2.8. Along both transects total Se is highest in the upper marsh and declines to less than 0.5 ppm in the mudflats. Although this is qualitatively a similar trend to the one for salinity (c.f. Figure 2.6), the high and low points for EC and Se do not exactly coincide, suggesting that the distribution of Se may be only weakly controlled by evapotranspirative redistribution. The reason for this becomes apparent upon examining the concentration and distribution of soluble Se, expressed as percentage of total (Figure 2.9). Soluble Se comprises on average 1% of the total inventory and even though the correlation between EC and soluble Se is fair, the low concentrations of dissolved Se will limit the extent to which Se can be re-distributed in the sediments.

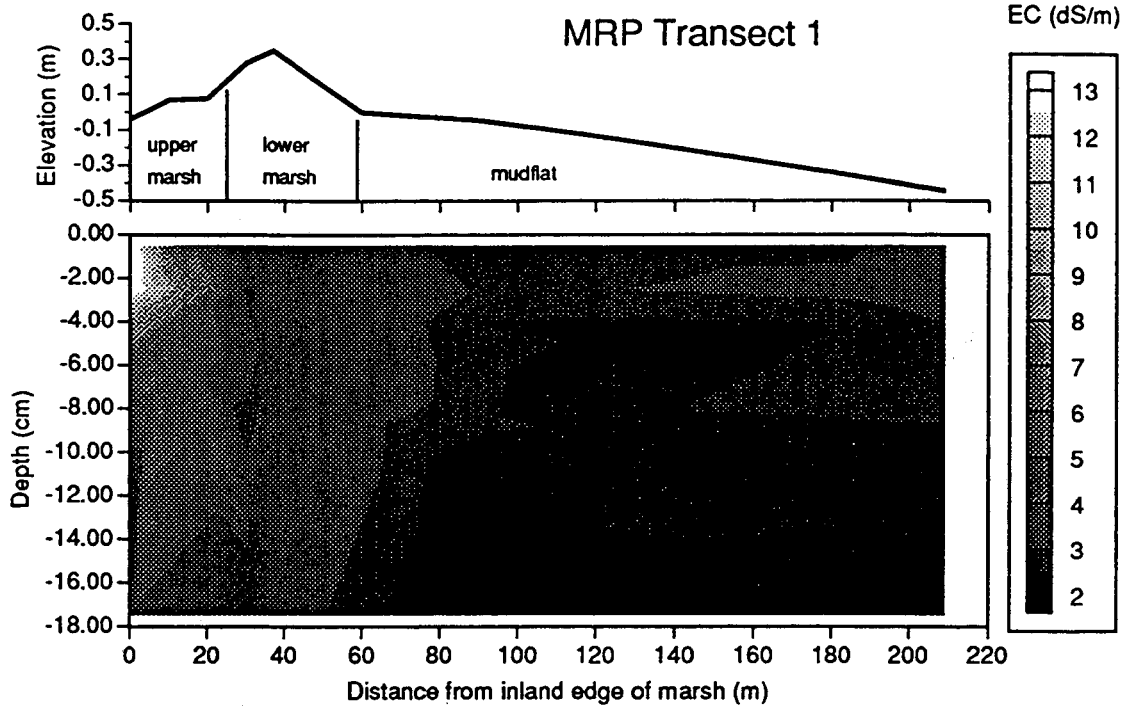

Figure 2.6 Electrical conductivity, measured along Transect 1 at site MRP. The top graph shows the surface elevation of the transect.

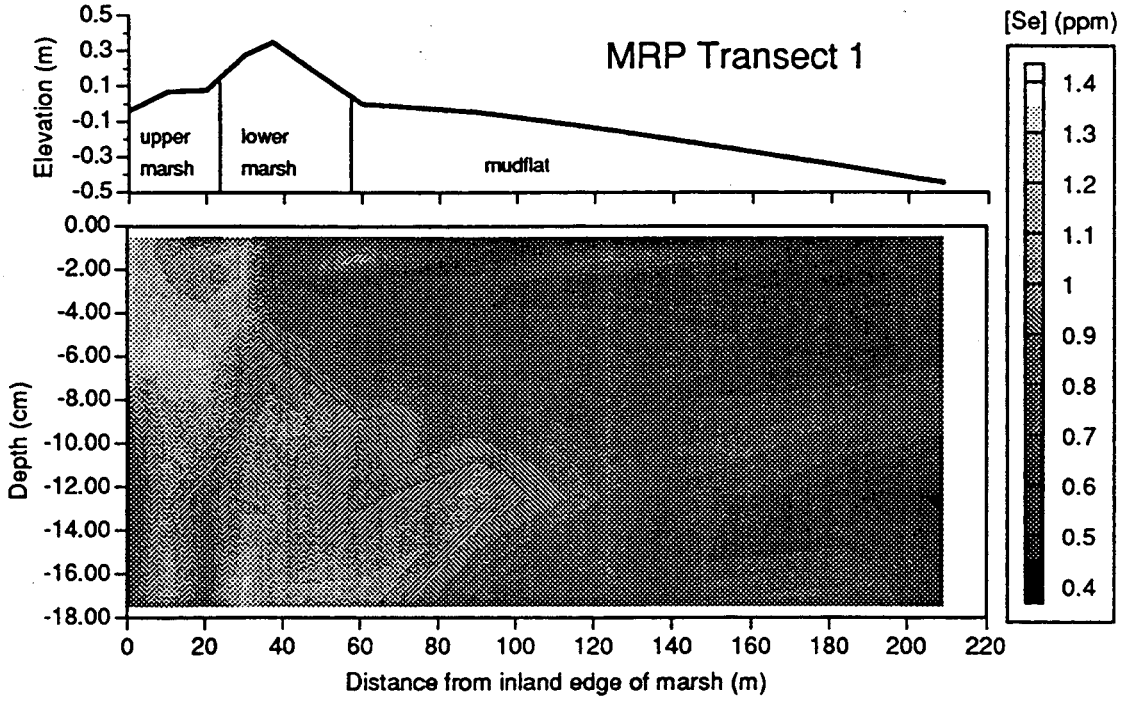

Figure 2.7 Total Se concentrations, measured along Transect 1 at site MRP. The top graph shows the surface elevation of the transect.

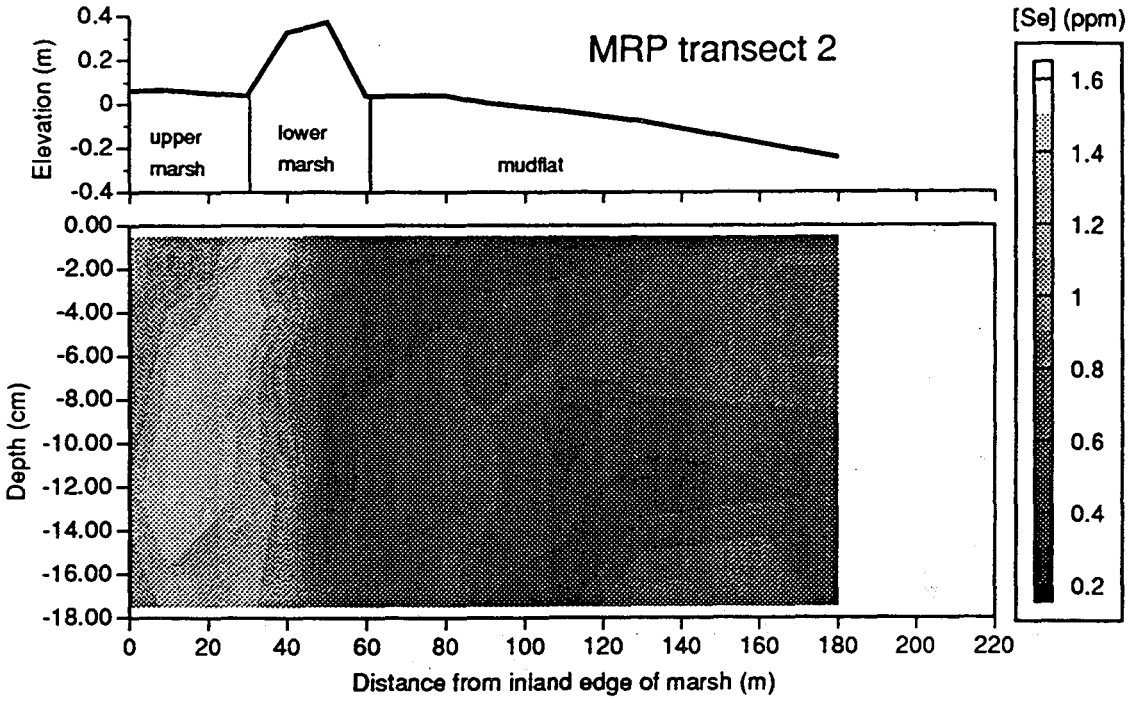

Figure 2.8 Total Se concentrations, measured along Transect 2 at site MRP. The top graph shows the surface elevation of the transect.

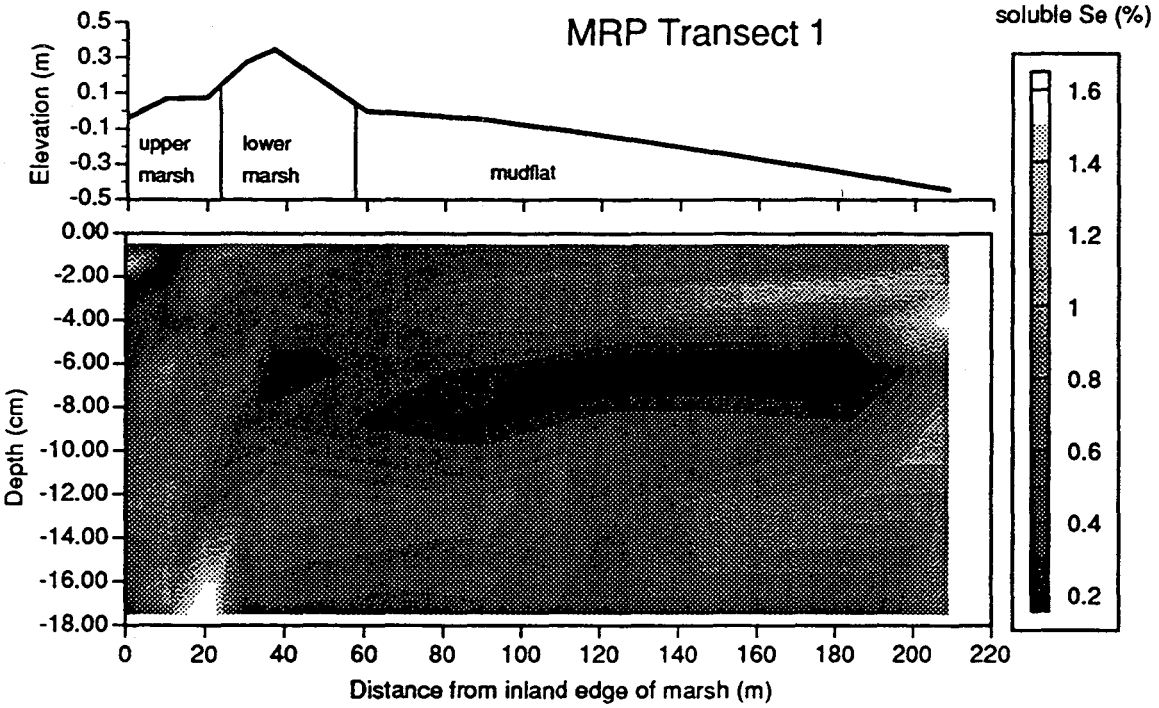

Figure 2.9 Soluble Se, expressed as percentage of total , measured along Transect 1 at site MRP. The top graph shows the surface elevation of the transect.

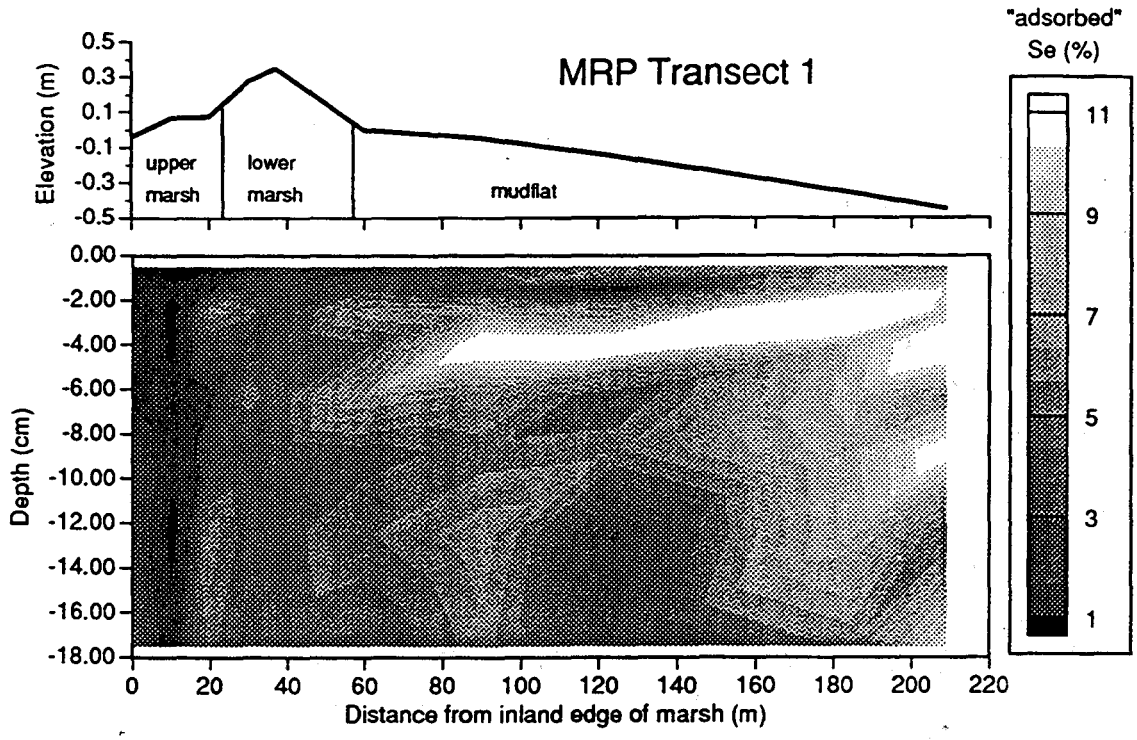

Figure 2.10 "Adsorbed" Se, expressed as percentage of total , measured along Transect 1 at site MRP. The top graph shows the surface elevation of the transect.

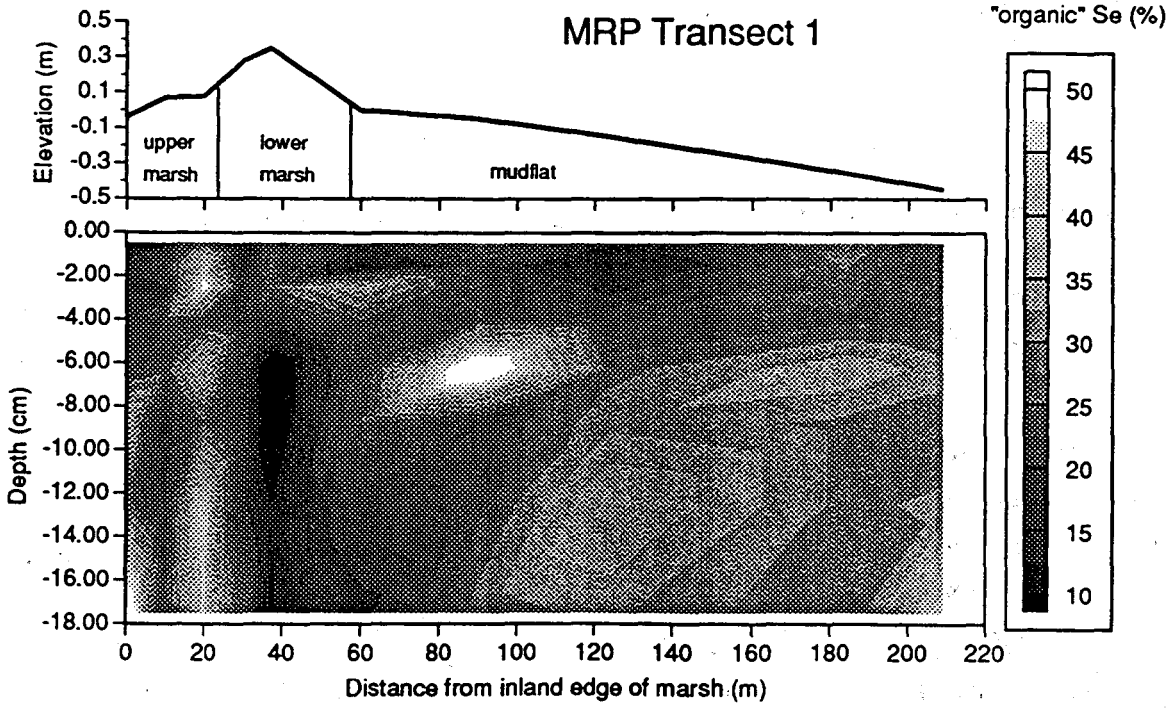

Figure 2.11 "Organic" Se, expressed as percentage of total , measured along Transect 1 at site MRP. The top graph shows the surface elevation of the transect.

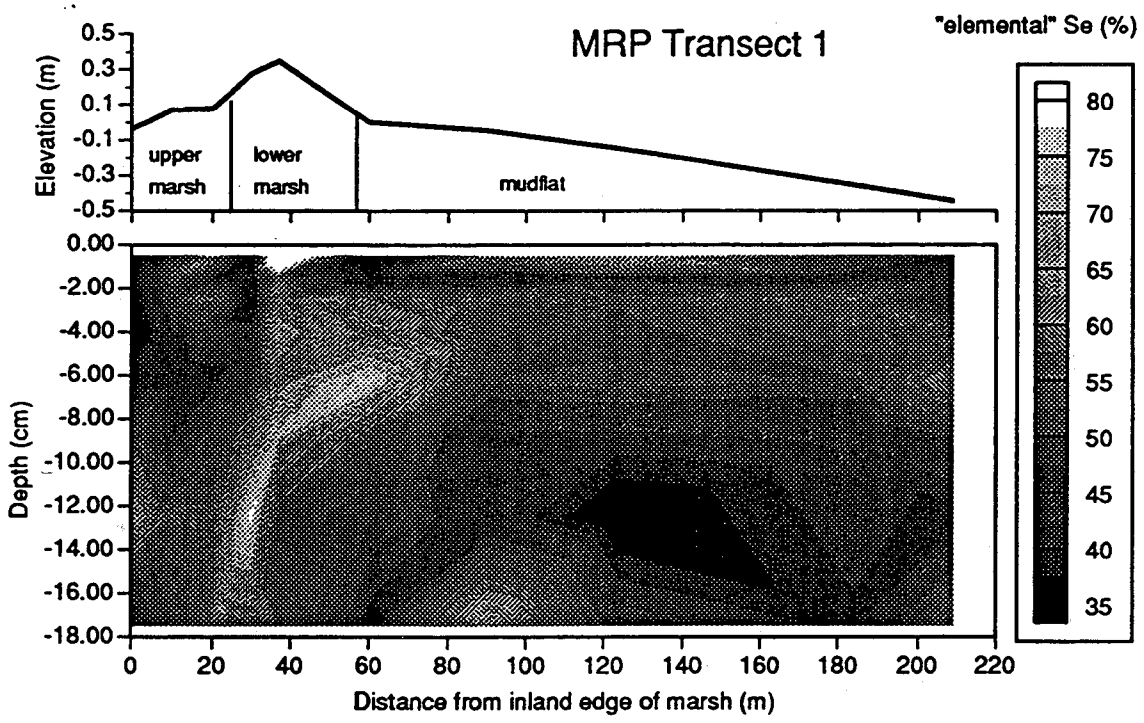

Figure 2.12 "Elemental" Se, expressed as percentage of total, measured along Transect 1 at site MRP. The top graph shows the surface elevation of the transect.

"Adsorbed" Se, primarily selenite, exhibited a weak positive correlation with environment, that is it comprised a larger percentage of total in the mudflats than in the marsh, and an as yet unexplained fair positive correlation with pH (Figure 2.10). This is contrary to numerous field and laboratory studies in which selenite adsorption decreases with higher pH, especially above pH 8 (e.g. Balistrieri and Chao, 1987; Neal et al., 1987).

"Organic" Se, which is likely a combination of Se adsorbed onto organic substances and Se in organic molecules, is shown in Figure 2.11. There are no significant trends, except localized zones in the lower marsh region. "Organic" Se comprises on average 30 to 35% of total. "Elemental" Se comprises on average 55 to 60% of total and is therefore the dominant fraction (Figure 2.12). Qualitatively, "elemental" Se tends to be slightly elevated when "organic" Se is depressed and vice versa; for example, the low "organic" Se zone in the lower marsh coincides with a high in the "elemental" Se. Together, these two fractions comprise no less than 50% and as much as 95% of the total Se inventory in the sediment.

3 SE IN SURFACE WATER AND SUSPENDED PARTICULATES

3.1 Surface Water Se

Dissolved Se concentrations for waters sampled from the Carquinez Strait at the MRP site waters were measured from November 7th, 1995 through June 19th, 1996 and are shown in Figure 3.1. Selenite numbers for the same samples are still being measured.

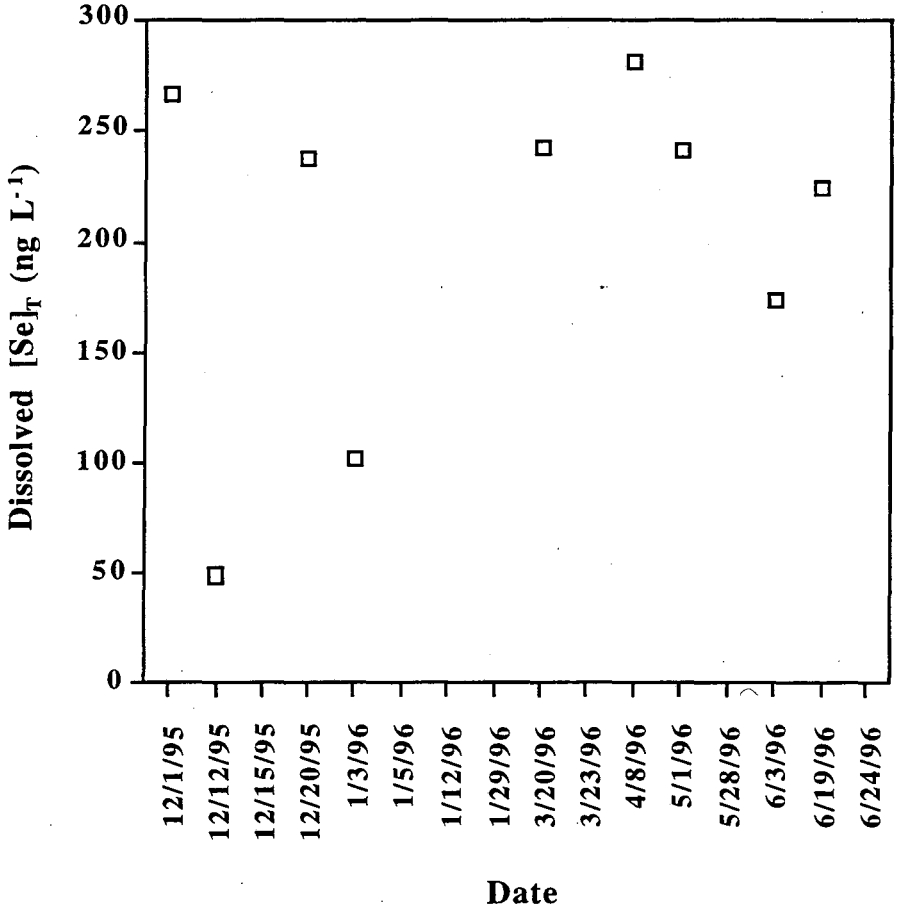

Figure 3.1 Total Se concentrations for surface water samples from the mudflats of Martinez Regional Park.

3.2 Suspended Particulate Matter Se

The sequential extraction procedure was modified for the low-mass suspended particulate matter (SPM) samples; Se was extracted using a similar series with the exception

of the use of a distilled water extract. The sequence used was sodium phosphate (Px), sodium hydroxide (OHx), and sodium sulfite (Sx) extracts in sequence, with solid:liquid ratios ranging around 40:1 or 50:1.

Preliminary results show Px and OHx methods remove low amounts of Se, and that both extract less Se from SPM than the underlying mudflat sediments. Figure 3.2 shows the breakdown of Se in one of the SPM samples which falls around the average of the current samples. Px + Dx extracted Se is only 1.4%, considerably lower than the 8% average observed for the same fractions found in the 0-1 cm mudflat samples at Martinez Regional Park. Removal of these fractions in two separate washes could account for part of the disparity, but the differences are too great to be accounted for by such a small contribution (approximately 3-5% versus 6-15%). OHx-Se was low as well, with an average value of approximately 15% versus 33% found in the 0-1 cm mudflat samples. Given that SPM is the source of most of the sediment found in the mudflats, it is surprising that the extractability of Se in the two types of sediments are so different. Clearly. more samples need to be extracted to confirm these findings.

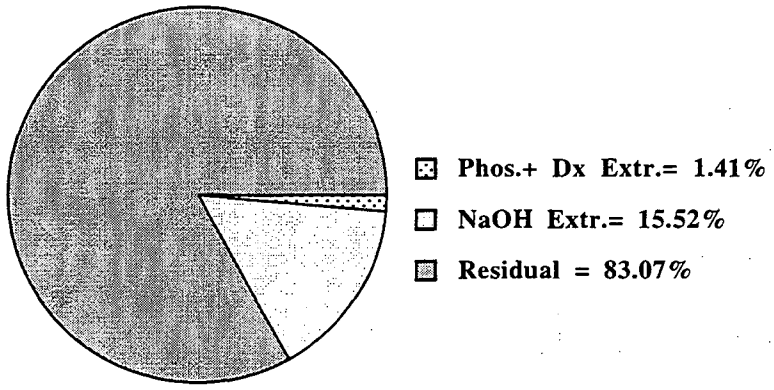

Figure 3.2 SPM-Se fractionation for sample 1/3/96 from the Martinez Regional Park site.

One reason for the differences may be the oxidation state of the environment. Surficial sediments in the mudflats are in a transition zone between a surface containing oxic waters and a subsurface zone where Se and other elements are being reduced. This transition zone is generally believed to be 2 cm thick, and this has been corroborated by the current study through redox potential readings of sampled columns (see Section 2.2.1). However, the lower readings of adsorbed and interstial Se in the SPM are not necessarily supported by the differences in the environments between the SPM and mudflat sediments. One line of reasoning which may explain the discrepancy is that surficial mudflat sediments

are in a zone where Se is adsorbed and reduced from selenate to selenite, and therefore more likely to adhere to surfaces. The greater concentration of OHx-Se in the mudflat sediments may also be a result of greater adsorption of selenite onto organic surfaces. The result is that metabolized Se in phytoplankton tissue is less significant in mudflats sediments than SPM.

Correlations between Se content overall or from particular fractions do not show high degrees of statistical significance (Figures 3.3, 3.4, and 3.5), and further sampling is needed to draw any valid conclusions.

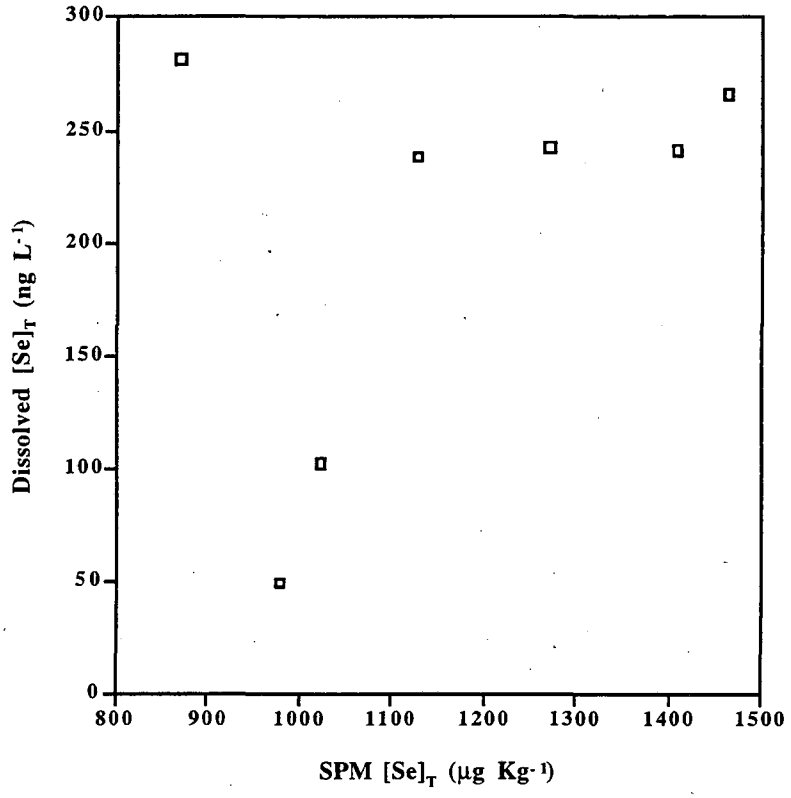

Figure 3.3 Concentration of total dissolved Se versus total SPM-Se.

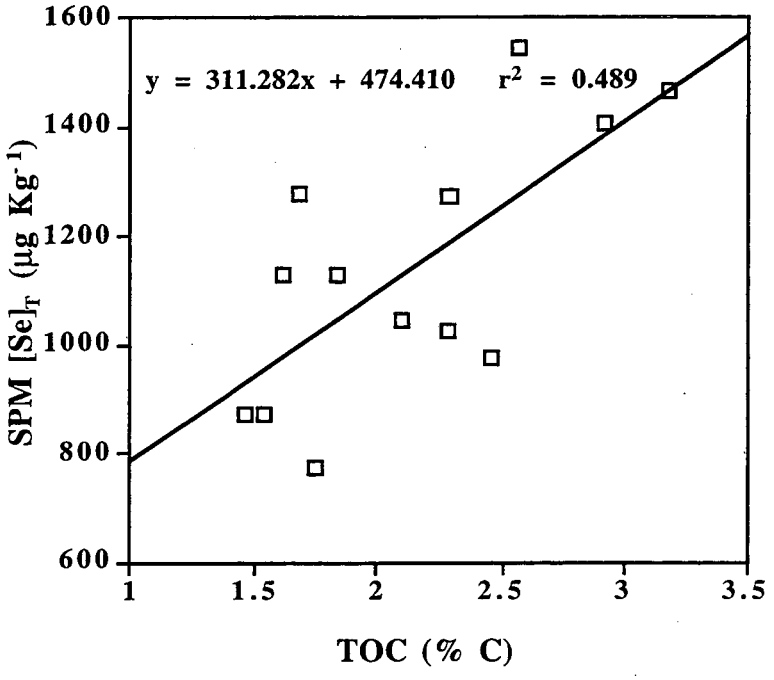

Figure 3.4 Concentration of total SPM-Se versus total organic carbon.

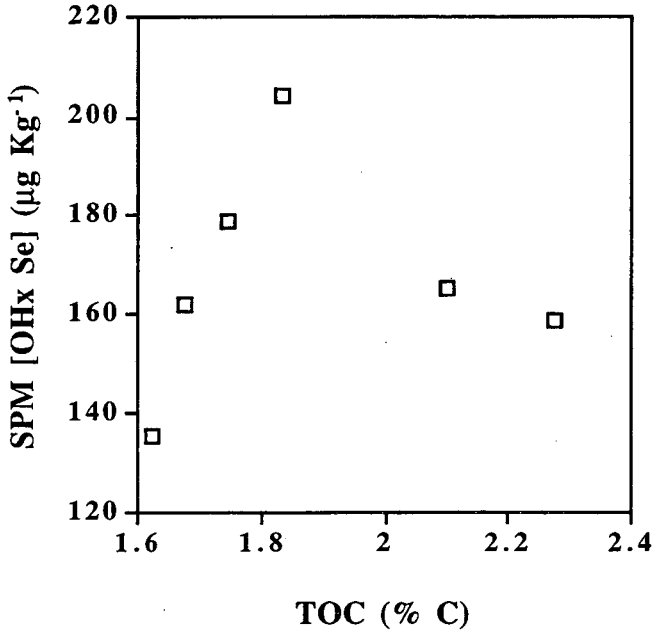

Figure 3.5 Concentration of SPM OHx-Se versus total organic carbon.

4 STABLE ISOTOPE METHODS

A second analysis of selenate from San Joaquin River water was completed. One liter of water collected at the I-5 crossing near Tracy was passed through an anion exchange resin to collect all of the anions, including selenate and selenite, from the water. Weak acids such as phosphate and organic acids (and also selenite) were then stripped from the column with dilute hydrochloric acid. The remaining anions, including selenate, sulfate, and chloride were then stripped from the column with 4 M hydrochloric acid. Because of the first stripping step, this solution contained little organic solute and little phosphate and this enhanced further processing. The 4M hydrochloric acid + sample solution was heated to convert the selenate to selenite and neutralized to pH 7. Then the usual ferric hydroxide purification process was carried out.

Table 4.1 is an updated compilation of analyses carried out to date. Based on the results of the Tracy water analysis, it appears that a systematic difference between refinery effluent selenium and river-borne selenium that would enable isotopic tracing of refinery effluent in the estuary may not exist. However, additional samples need to be analyzed to confirm these results.

Table 4.1. Se isotope ratios of refinery effluent and river water.

Sample	80Se/76Se ratio	d80Se (per mil)
Chevron Effluent	5.3198	+4.4 ±1
Shell Effluent	5.3229	+4.9 ±0.4
Unocal Effluent	5.3134	+3.2 ±0.4
Exxon Effluent	5.3249	+5.3 ±0.2
San Joaquin R. near Tracy	5.3106	+2.6 ±1
Antioch Water	5.3258	+5.5 ±1

4.1 Selenium extraction and purification

4.1.1 Hydride generation as a purification procedure

Hydride generation was avoided as a purification method early in this project because the rapid reduction inherent in the method could greatly alter the isotope ratios of the

processed samples. However, we have successfully corrected for similar bias introduced by the mass spectrometer using the double spike technique. As long as the spike is introduced before purification procedures, alteration of the selenium isotope ratios during purification can be corrected for along with the mass spectrometry bias.

The hydride generation method is the same as that used for low-level selenium analysis, and will enable relatively rapid processing of sediment extracts and digests. The sample solution is mixed with hydrochloric acid, sodium borohydride is added, and the evolved hydrogen selenide is swept from the solution by a carrier gas. For isotope ratio analyses, the hydrogen selenide is absorbed in nitric acid. This solution is then easily prepared for mass spectrometry because there are few other elements other than selenium in it.

An absorption tube, in which the carrier gas and hydrogen selenide are bubbled through the nitric acid, was fabricated and was tested to verify that complete absorption was obtained. Then, the MH495 standard was spiked and processed through the hydride apparatus and analyzed on the mass spectrometer. As expected, the double spike method successfully compensated for any alteration of the 80Se/76Se ratio, and the correct value was obtained for the standard.

4.1.2 Removal of organic molecules from solutions

Successful removal of organic molecules from solutions during selenium purification was attained using hydrogen peroxide. A few experiments showed that this treatment oxidizes selenite to selenate very rapidly in basic solutions, but does not oxidize selenite to selenate in the acidic solutions used in the standard purification procedure. These findings were very useful in removing organic molecules and also in controlling the oxidation state of selenium during the processing.

4.1.3 Decreasing the required sample size for mass spectrometry

The technique for amplifying the output of the ion beam detector was investigated. It was found that precise results (less than 0.5 per mil uncertainty) can be obtained on many samples, but a consistent offset of +3.5 per mil was observed. Our collaborator at the USGS, Tom Bullen, is investigating this odd result, but in the meantime analyses of small samples that produce weak ion beams can be carried out. The offset can be subtracted from the results to yield a reasonably accurate analysis (±1 per mil).

5 PROGRESS ON ANALYTICAL METHODS DEVELOPMENT

5.1 Liquid Nitrogen Trapping Low-Level Se Analysis Method

In an effort to improve the reliability and the utility of the Cutter L-N_2 Se trapping method, we improved the extent of silanization and changed a variety of procedures:

1. Increased the length of time used for silanization.
2. Kiln cleaned all glassware prior to silanization.
3. Solvent washed all glassware with toluene, hexane, and methanol prior to water washes. Used no acid or detergent for washes.
4. Never used a standard with a concentration greater than 5 ng on a regular basis.
5. Ran blanks between every standard and sample (until baseline returned to less than 300,000 area units.
6. Cooled all samples prior to running.
7. Washed the water trap and bubbler with water after every seven samples, and ran blanks after cleaning to verify baseline readings.

With these changes in the operating procedures, we observed a quantification limit of 0.5 ng with a variance in the standard deviation to average ratio of less than 20%. Measurements could be made below 0.5 ng, but double blanks must be run between samples, and the water trap would require cleaning more often than after every seven samples. At the current flow rate (225 mL min^{-1}) the water trap accumulates water rapidly. HCl also appears to accumulate in the water trap along with trace quantities of Se as H_2Se. The H_2Se is released after washing, and appears to be released by hydride generation. It is unclear why washing and drying the water trap does not release this selenium. A better understanding of how the Se is trapped in the system would aid in the optimization of analysis conditions. At present it is obvious that a trace amount of every sample is left in the system, making the system inefficient. Fortunately Se is trapped at a constant rate making quantification possible.

5.2 FIAS Low-Level Selenium Analysis Method

The FIAS procedure for low level selenium analysis has been further developed to examine the matrix effects that will be observed when analyzing brackish and seawater samples. The main objectives were to:

1. Gain more insight into the design of the knotted reactor.
2. Optimize the system for maximum absorbance for the minimum amount of sample.
3. Examine the effects of anions on co-precipitation.
4. Examine the effects of organic compounds in Bay waters on spike recovery.

The knotted reactor is used to catch the $La(OH)_3$/Se(IV) precipitate that forms in solution. The way the knots are tied is critical to the overall sensitivity of the system. We observed a significant sensitivity increase following a redesign of the reactor, based on discussions with E.H. Hansen, the originator of this reactor design. Currently, for a 25 second load time, a 1.0 abs for a 1 mg/L sample is observed. Previously, a 70 second run time gave a 0.7 abs for a 1 mg/L sample.

The optimization of the system was another high priority. The modifications to the system were small but significant. Three knotted reactors were set up in parallel to give a more efficient trapping and larger signal. Lowering the buffer flow rate resulted in increased sensitivity, as was also observed by Nielsen et. al. (1996). The argon flow was lowered to 75 mL/min. Lastly, the buffer pH was set to 9.10 and was made by mixing a 1:1 ratio of 0.2 M NH_4Cl + 0.2 M NH_4OH. Of these changes, the argon flow rate change was the most significant. The peak shape changed drastically giving a taller and sharper peak. This allowed the software to integrate the peak more consistently and took out the effects of random noise in the baseline. After making these changes, blank levels decreased to 0.002 abs, thereby increasing confidence in measurements at the lower end of the spectrum. A detection limit study was performed on a 1 mg/L standard with a 25 sec load time and at 3s the absorbance was 0.012 and a minimum detection limit of 0.009 mg/L, or 9 pptr. This calculates back to a quantitation limit of 0.031 mg/L.

The prevention of carry over is another problem. It was noted that there is roughly 14% carryover in sample analysis. This was reduced to 2% with a 20 second wash with 0.1 M HCl between samples.

The next phase was to examine the anion effects on coprecipitation efficiency. The anions most commonly found in seawater matrices are: chloride, sulfate, nitrate, and phosphate. Nitrate and phosphate are primarily the cause of industry discharge or agricultural runoff. Ion chromatography analysis of water from Martinez has shown the presence of chloride and sulfate, but has not shown a significant amount of nitrate or phosphate. Analysis of water from Antioch showed the presence of chloride, sulfate and phosphate. From this data, a series of experiments was designed to see how much the coprecipitation would be hindered by the presence of these anions, starting with the effect of chloride concentration on coprecipitation. A 1 mg/L selenium standard was prepared in 4, 0.5, and 0.1 M NaCl solutions. For these concentrations the selenium loss was 20%, 12% and 3%, respectively. The effect of sulfate on the system was examined at sulfate concentrations of 0.1 and 0.01 M Na_2SO_4. For these concentrations the selenium loss was 70% and 10%, respectively. The effect of phosphate on the system was examined at phosphate concentrations of 1.0 and 0.1 mM Na_3PO_4. For these concentrations the selenium loss was 100% and 83%, respectively. The effect of nitrate on the system was examined at nitrate concentrations of 1.0 and 0.1 M $NaNO_3$. For these concentrations the selenium loss was 28% and 3%, respectively. These results are summarized in Table 5.1.

Table 5.1 Anion concentrations needed to reduce FIAS-Se sensitivity by 10% or 20%.

Percent Loss of Selenium	@ Phosphate mg/L	@ Sulfate mg/L	@ Chloride mg/L	@ Nitrate mg/L
10 %	1.14	960	37700	21800
20 %	2.28	1920	75400	43600

This table clearly demonstrates that moderate levels of phosphate in the sample will prevent the coprecipitation of selenium with the $La(OH)_3$. Water from Martinez has chloride and sulfate present, but does not have measureable phosphate or nitrate. The presence of phosphate in Antioch suggests the need to establish corrections for anion interference in Carquinez Strait samples.

The effects of organic compounds in Martinez water were examined. When Martinez water was spiked with 1 mg/L of selenite and analyzed directly, the recovery was 61%. In order to assess the influence of organics on the recovery, organics needed to be removed from the sample, which was done with either hydrogen peroxide or persulfate. When 50 mL samples were treated with 0.5 mL of peroxide, selenium recoveries averaged around

20%. When the samples were treated with 0.5 mL of persulfate and heated the recovery was 62%. When 2.5 mL of persulfate was added to 50 mL of seawater, the recovery improved to 75%. Apparently, the remaining 25% loss in sensitivity is due to anion effects. This lends further importance to understanding anion interference and improving the correction curves for chloride and sulfate. Routine analysis of anions in order to correct for anion interference may be required. A direct comparison between the cold-trap and FIAS methods should shed light on the sensitivity of both methods.

6 SEDIMENT DYNAMICS

As described in a previous Quarterly Progress Report (Zawislanski et al., April 1996), the sediment budget for sites MRP and SHB is being quantified in order to estimate (1) the impact of suspended particulates on Se deposition and (2) the significance of re-suspension on bottom sediment transport, which could potentially have an impact on the bio-availability of Se-enriched sediment. Figure 6.1 illustrates the many pathways that suspended sediment can follow throughout a marsh. Hopefully, it will be possible to measure the fluxes along each pathway to develop a complete sediment budget at Martinez Marsh. Ideally, one would like to be able to model these pathways so that this budget will be a general one that can be applied elsewhere.

6.1 Modeling Sediment Transport

Sediment is brought into the estuary by the combined flows of the San Joaquin and the Sacramento rivers. During flood tides, the suspended sediment is brought up onto the marsh. When the flow velocity is sufficiently low (e.g. during slack tide), these particles may settle out of suspension and be deposited. The residence time of these particles is determined by the rate of resuspension. Most studies indicate that tidal flows do not develop the shear stress necessary to resuspend sediment. Waves, on the other hand, can develop significant shear stresses.

Analytically, there are only two physical processes that need to be quantified. The first is the bottom shear stress caused by the waves. When the bottom shear stress is greater than the shear strength of the sediment, sediment transport occurs. The shear stress can be expressed as a function of wave height and period (Madsen 1976 as cited by Hawley and Lesht, 1992):

$$\tau_b = \frac{H\rho\upsilon^{0.5}(2\pi/T)^{1.5}}{2\sinh(2h\pi/L)}$$

where H is the wave height, T the wave period, L the wave length (derived from T), ρ the density of water, h is water depth, and υ the kinematic viscosity of water. Since wave

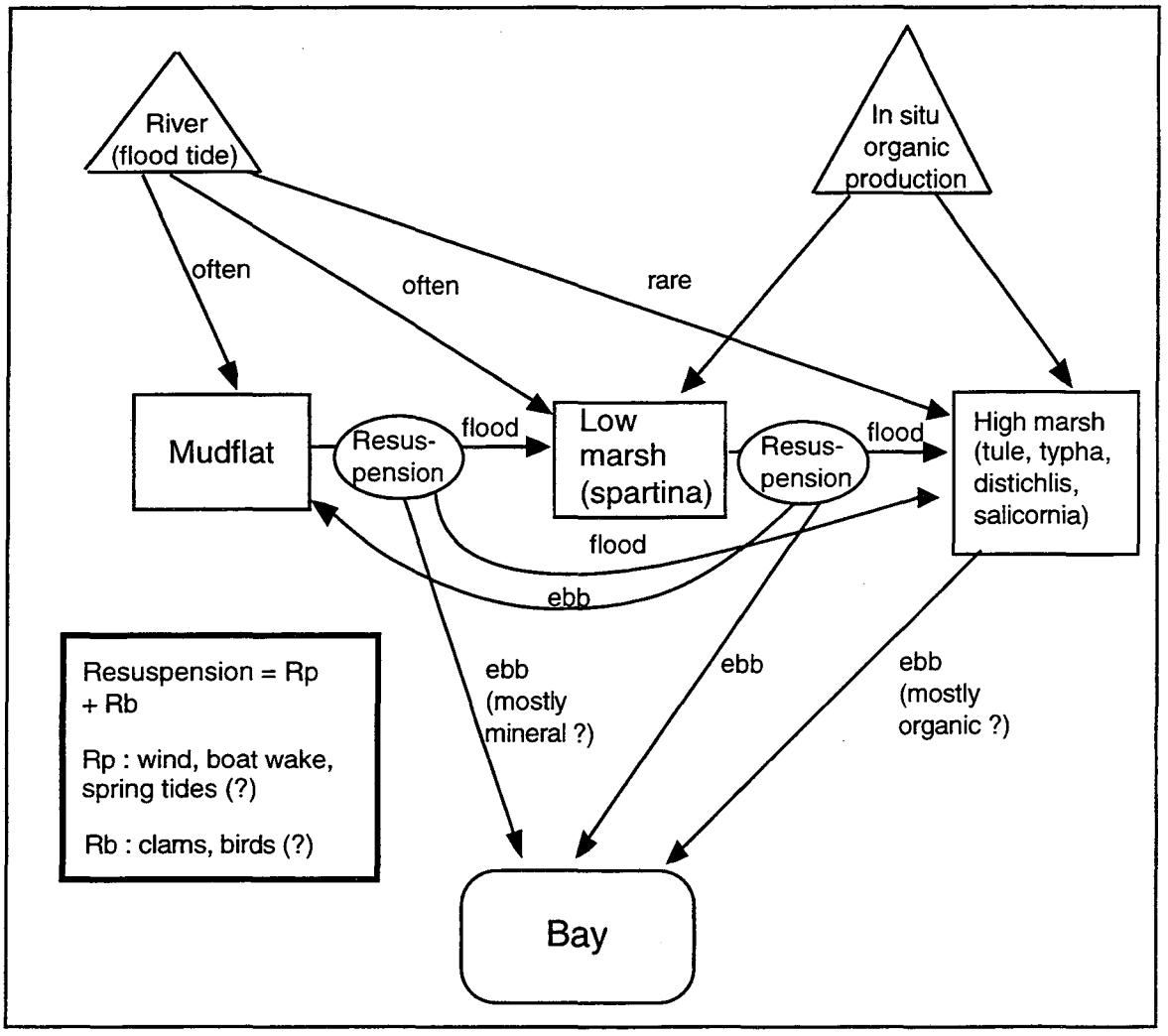

Figure 6.1 Flow chart showing different pathways that sediment can follow through the intertidal zone.

height and period are dependent on wind velocity, fetch, and water depth (which is a function of the tides and discharge), it should be possible to predict the conditions necessary to cause resuspension. Unfortunately, the shear strength of the sediment is very difficult to calculate because of the physico-chemical interactions between the individual grains. Previous studies have measured strengths ranging from 0.7 to 3.6 dynes cm^{-2} for estuarine sediments, however there is no way to know if these numbers are appropriate for Martinez Marsh. Some simple flume studies may be necessary to measure the shear strengths.

The second important process is the settling of the sediment. This is primarily dependent on two variables: flow velocity and particle size. Flow velocity will be affected by tidal currents, wave motion, and form drag. Form drag is caused by the vegetation and can significantly slow the movement of water and create back-eddies that induce sedimentation.

6.2 Preliminary Data

Data from sediment traps laid in a transect from the mudflat up to the high marsh provides information on sedimentation rates that can be used to verify and calibrate the sediment budget model (Figure 6.2). This data also shows some interesting seasonal

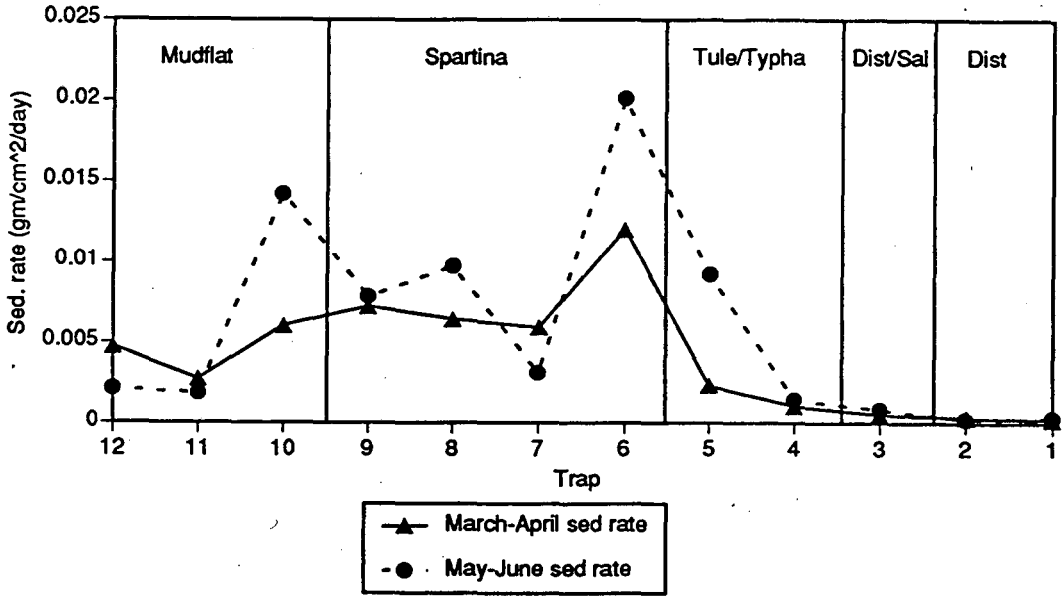

Figure 6.2 Spring sedimentation rates measured at Martinez Regional Park.

changes in sedimentation. In general, rates on the mudflat and low marsh in May and June are higher than the rates in March and April. This is surprising since the higher suspended sediment concentrations, greater discharges, and storm surges during the earlier months would be expected to result in higher sedimentation rates. However, a dramatic rise in biological activity at the end of spring would increase the rates of bio-flocculation. Furthermore, as the upstream discharge of freshwater decreases, flocculation may increase with the rise in salinity. Clearly, the lowest rates of sedimentation occur in the upper marsh

(traps 1,2, and 3). Preliminary total Se data (not shown) suggest that particulates deposited in the upper marsh contain two to three times as much Se as those deposited on the mudflat. Further sampling and analysis are needed to confirm these observations.

7 SELENIUM SPECIATION OF BIOLOGICAL MATERIALS

A preliminary investigation to identify Se speciation in biological materials was conducted using high resolution, in-situ X-ray absorption spectroscopic (XAS) techniques, which have been proven to be versatile in distinguishing different trace element forms in a variety of samples (Brown *et al.*, 1988). Using X-ray absorption phenomena, it is possible to obtain information on local structure (EXAFS spectroscopy), oxidation state (XANES spectroscopy) and spatial distribution (X-ray microprobe) of the X-ray absorbing element without significantly disturbing or modifying the original sample. The element-specific chemical information can be obtained from either bulk or from selected small regions (linear dimensions ranging from 1 μm and up to 1 mm, for micro-XANES) of a sample. The synchrotron X-ray microprobe permits 2-dimensional elemental concentration mapping with spatial resolution as fine as 2 μm (Jones and Gordon, 1989) and concentrations as low as 1 ppm. Using these techniques we intend to identify different Se species and their chemical form in the biota of the San Francisco Bay-Estuary waters and sediments. For this preliminary investigation, we used clam samples (*Potamocorbula amurensis*, collected from Martinez Bay) supplied by Sam Luoma and his colleagues (USGS, Menlo Park, CA).

7.1 Methods

The clam sample collection, cleaning and preservation procedures are described in Luoma *et al.* (1989). The clam tissue was separated from shells and transported to the synchrotron facilities in frozen condition. For bulk XANES spectra, the tissue of all the collected clams was positioned in between two mylar windows and mounted on a photographic slide. Se K-edge XANES spectra were collected in fluorescence mode (13-element array detector) at the Stanford Synchrotron Radiation Laboratory, Stanford, CA, on Beamline 4-3 with Si (220) monochromator crystals. The resolution at the Se K- edge was better than 0.4 eV. Spectra were collected for different Se-containing inorganic (metallic Se, SeO_4, SeO_3, selenide) and organic compounds (seleno-cystine, seleno-methionine) (Figure 7.1). The energy position of the clam sample and these model compounds were calibrated against a Se(0) foil. Single scans were collected for all of the samples in the energy range of 12430-12770 eV, with a step size of 0.2 eV adjacent to the edge region.

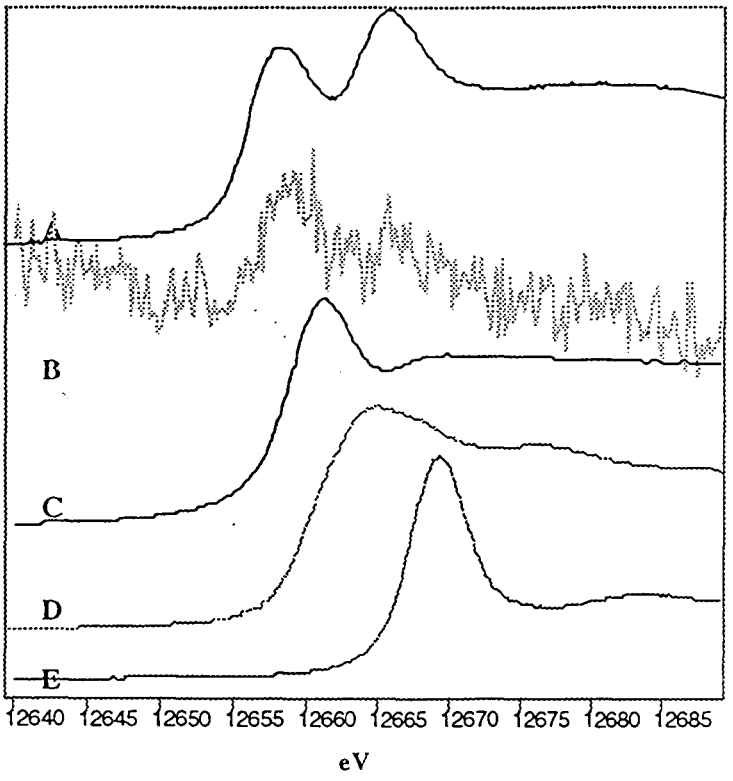

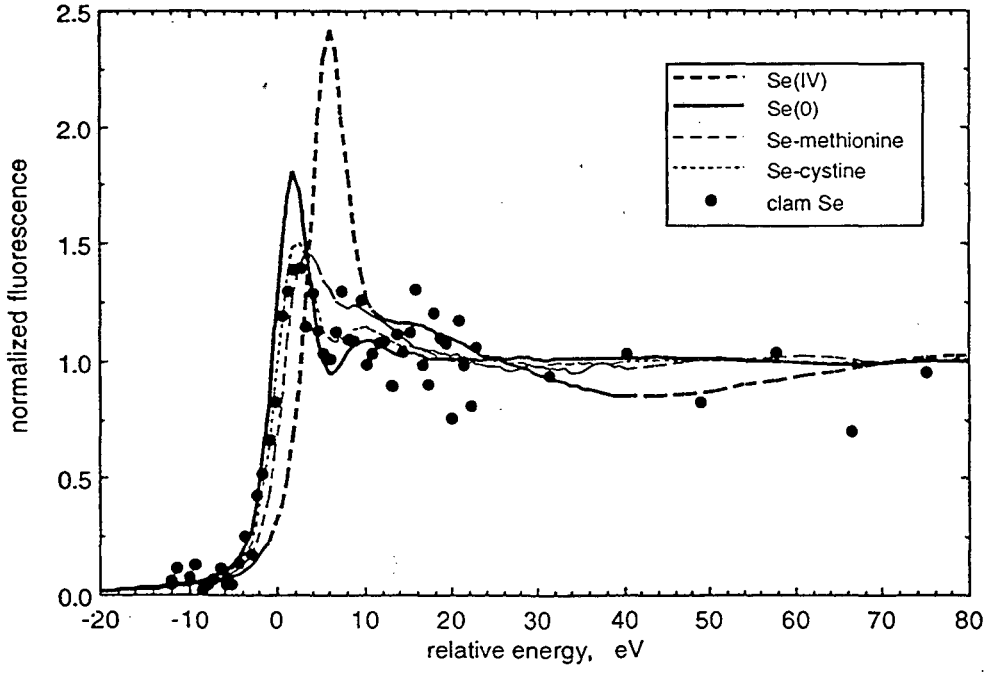

Figure 7.1 a. Se K-edge XANES spectra of bulk clam sample. The spectra shown here are of A. selenide, B. clam Se, C. Se (0), D. seleno-methionine, and E. selenate; b. Micro-xanes spectra of clam-Se collected from a selected location in the gut.

The micro-XANES studies were conducted at the National Synchrotron Light Source (Brookhaven National Laboratory, Upton, NY) on synchrotron microprobe beamline X26A. Operating characteristics of this facility are described in Sutton et al. (1995). For the present work, synchrotron X-rays were passed through a channel-cut monochromator and ellipsoidal focusing mirror, without additional collimation. The effective beam size was about 0.3 mm. The clam was positioned such that the incident X-ray beam was focused on the more dense, central region containing major organs (Figure 7.2a). The monochromator was tuned from about -50 eV to about +100 eV relative to the Se(0) K absorption edge (taken as 12658 eV), in steps ranging from 0.7 eV (in the near- edge region) to 9 eV.

The clam Se mapping data were collected on an X-ray microprobe, with monochromatic X-rays tuned above the Se K-edge focused onto the sample. A stepper motor-driven x-y stage is used to scan the sample in front of the stationary x-ray beam, and fluorescent x-rays emitted from the targeted spot are detected with an energy-sensitive detector. The beam characteristics have been described previously. The elemental map was generated by scanning across a 16 X 13 mm area in a 0.5 mm grid, with about 40 s at each spot.

7.2 Preliminary Results

K-edge XANES spectra of different Se containing compounds are shown in Figure 7.1, and the edge positions of these samples agree with the reported XANES spectra (Pickering *et al.*, 1995). The model compound XANES spectra indicate that the energy position of edge increases linearly with increases in Se oxidation state. Of the examined model compounds Se (-II) has the lowest energy, SeO_4 has the highest energy, and the rest are in between these two. Seleno-cystine and -methionine have energies in between Se(0) and SeO_3. In addition to the energy position, the XANES spectra 10 eV above the edge also exhibit structure, which is a function of the local coordination around Se atoms (Figure 7.1). When compared to these Se-models, Se-edge spectra of the clam sample is very noisy due to its low Se concentration. In addition, only a single scan was collected from this clam sample. However, the edge position of clam-Se is distinctly different from the rest of the examined models. The effective oxidation state of Se in clam may be less than (0) but greater than (-II). This form of Se is the dominant fraction in clam tissue, and this does not rule out the possibility of existence of other Se forms which may be in relatively smaller percentages. However, more data is required to establish Se-speciation in clam.

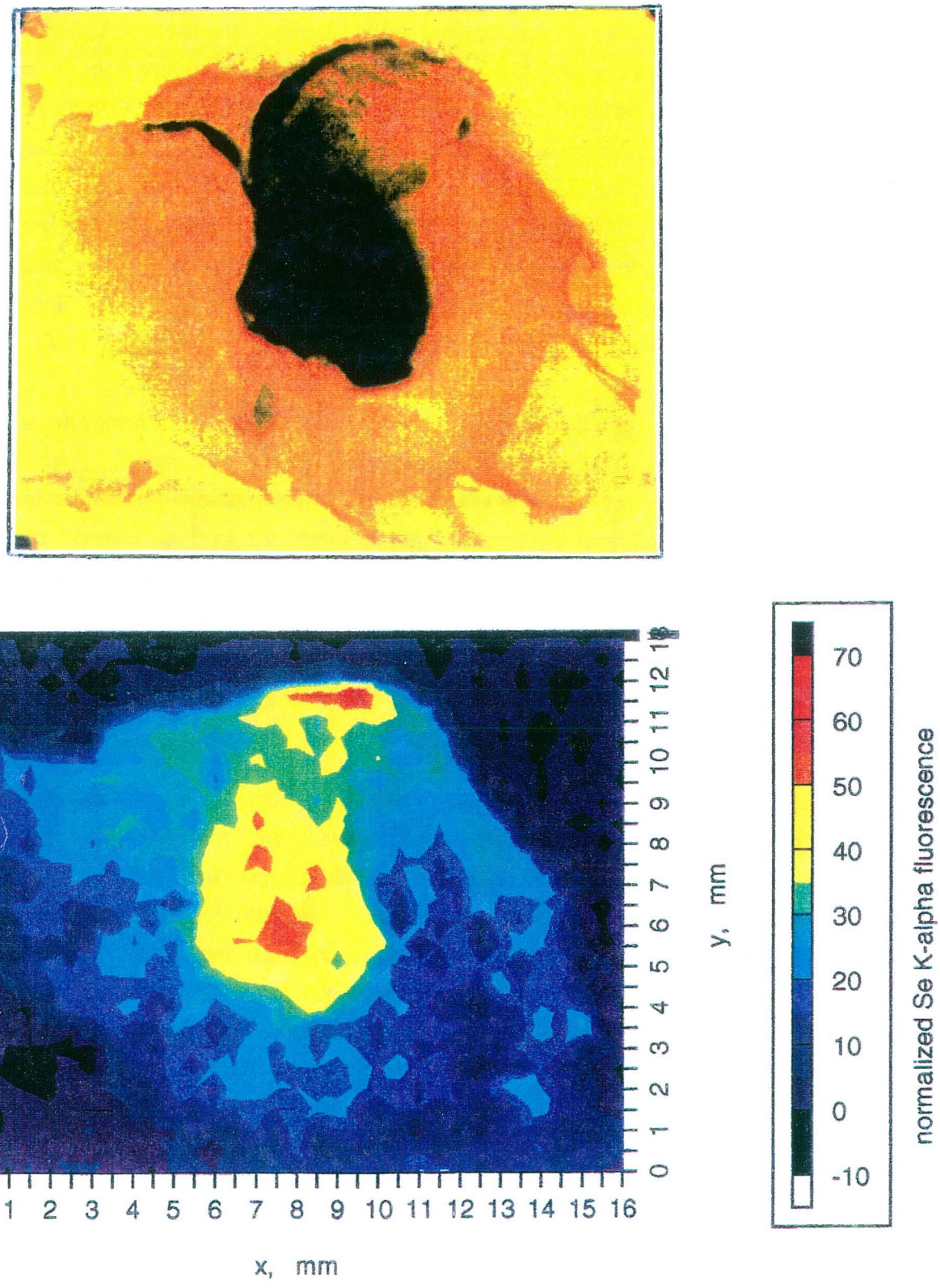

Figure 7.2 a. (top picture) Optical micrograph, and b. (bottom picture) X-ray microprobe Se mapping of Potamocorbula amurensis.

Se K-edge was clearly discernible in the micro-XANES scan (Figure 7.1b), but experimental problems associated with the monochromator energy calibration prohibited the accurate Se oxidation state determination. An energy uncertainty of about ± 1 eV was noted from periodic testing of standard samples. The qualitative features of the absorption edge are preserved, and these indicate that neither SeO_3 nor SeO_4 are present in significant (> 10%) proportions.

Relative concentration maps were prepared for different elements in the clam sample, but only Se data is presented here. The false-color map (Figure 7.2b) displays normalized Se K-α fluorescence count intensities (proportional to detected Se 2p to 1s electronic transitions). It should be noted that variations in sample thickness and matrix composition also contribute to apparent concentration contrasts, and such effects are expected to yield up to about 3-fold differences within this sample. Nevertheless, this map indicates that Se is largely concentrated in the central organs (gut), and to some extent also in the region tentatively identified as the intestine. The mantle has relatively much smaller Se concentration. This clearly indicate that Se-accumulation is dominant in certain organs of the clam and such distribution may relate to the food ingestion rates and Se residence time in clam, which have to be further examined.

7.3 Future Study

This feasibility experiment indicates that synchrotron XANES and X-ray microprobe analyses can serve as very useful tools in studies of trace element uptake and transformations in *P. amurensis* and other organisms. It is worth noting that the size of *P. amurensis* (~10 mm) is practically ideal for x-ray microprobe analyses. In larger organisms, dissection and conventional chemical analyses of separated tissue and organs is needed. Differentiating elemental distributions within much smaller organisms would probably require thin-sectioning, which can result in substantial sample distortion and possible redox transformations of some target elements.

For future in-depth study, samples of different clam species, and algae are collected from several locations in the San Francisco Bay. We are also obtaining fish and bird tissues for similar studies and the Se-speciation of these higher organisms will be compared with those of algae, and clams. This study may help identifying the Se-species causing biomagnification.

8 REFERENCES

Balistrieri L.S. and T.T. Chao. 1987. Selenium adsorption by goethite. Soil Sci. Soc. Am. J. 51:1145-1151.

Brown Jr. G.E., G. Calas, G. A. Waychunas, and J. Petiau. 1988. X-ray absorption spectroscopy: Applications in mineralogy and geochemistry. In Spectroscopic Methods in Mineralogy and Geology. Ed. F.C.Hawthrone. Rev. in Mineral. 18, Mineral. Soc. Am. 431-512.

Cutter, G. A. 1978. Species determination of selenium natural waters. Analytica Chimica Acta, 98: 59-66.

Cutter, G. A. 1989. The Estuarine Behavior of Selenium in San Francisco Bay. Estuar. Coast. Shelf Sci. 28:13-34.

Ganje and Page. 1974. Rapid acid dissolution of plant tissue for cadmium detrmination by atomic absorption spectrometry. Atomic Absorb. Newsl. 13:131-134.

Jones, K.W., and B. Gordon. 1989. Trace element determinations with synchrotron-induced x-ray emission. Anal. Chem. 61:341A- 358A.

Luoma, S., C. Johns, N. Fisher, N. Steinberg, R. Oremland, and J. Reinfelder. 1992. Determination of selenium bioavailability to a benthic bivalve from particulate and solute pathways. Environ. Sci. Tech. 26:485:491.

Madsen, O.S. and W.D. Grant. 1977. Quantitative description of sediment transport by waves. In: Proceedings o the 15th Coastal Engineering Conference, 2:1093-1112.

Neal, R.H., G. Sposito, K.M. Holtzclaw, and S.J. Traina. 1987. Selenite adsorption on alluvial soils: I. Soil composition and pH effects. Soil Sci. Soc. Am. J. 51:1161-1165.

Nielsen, S., Sloth, J.J., and Hansen, E.H., Analyst, vol. 121, 1/96, pp. 31-35

Pickering, I. J., G. E. Brown Jr., and T. K. Tokunaga. 1995. Quantitative Speciation of Selenium in soils using X-ray Absorption Spectroscopy. Env. Sci. Tech., V 29, 2456-2459.

Sutton, S.R., S. Bajt, J. Delaney, D. Schulze, and T. Tokunaga. 1995. Synchrotron x-ray fluorescence microprobe: Quantification and mapping of mixed valence state samples using micro-XANES. Rev. Sci. Instrum. 66:1464-1467.

Tao, G. and E.H. Hansen. 1994. Determination of ultra-trace amounts of selenium (IV) by flow injection hydride generation atomic absorption spectrometry with on-line preconcentration by coprecipitation with lanthanum hydroxide. Analyst. 119:333-337.

Zawislanski, P.T., S.M. Benson, A.A. Brownfield, E. Gabet, A.F. Haxo, T.M. Johnson, A.E. McGrath, H.S. Mountford, S. Myneni, J. Oldfather, T.C. Sears and H.-W.C. Wong. 1996. Selenium fractionation and cycling in the intertidal zone of the Carquinez Strait. Unpublished Quarterly Progress Report to the SFRWQCB and DOE. April 1996.

Zawislanski, P.T., A.E. McGrath, S.M. Benson, H.S. Mountford, T.M. Johnson, S. Myneni, L.Tsao, J. Oldfather, A.F. Haxo, and T.C. Sears. 1996. Selenium fractionation and cycling in the intertidal zone of the Carquinez Strait. Unpublished Quarterly Progress Report to the SFRWQCB and DOE. January 1996.

Zawislanski, P.T., A.E. McGrath, S.M. Benson, H.S. Mountford, T.M. Johnson, L.Tsao, J. Oldfather, A.F. Haxo, and T.C. Sears. 1995. Selenium fractionation and cycling in the intertidal zone of the Carquinez Strait. Unpublished draft Annual Report to the SFRWQCB and DOE.

Ernest Orlando Lawrence Berkeley National Laboratory
One Cyclotron Road | Berkeley, California 94720

Prepared for the U.S. Department of Energy under Contract No. DE-AC03-76SF00098